Technical Report

Crack Propagation in 3-D Printed PLA: Finite Element Modeling, Test Bed Design, and Preliminary Experimental Results

Albert E. Patterson

Department of Industrial and Enterprise Systems Engineering

University of Illinois at Urbana-Champaign

Abstract

The present study was a preliminary exploration of crack propagation in 3-D printed polylactic acid (PLA), a bio-mass generated recyclable polymer with excellent mechanical properties and many consumer and industrial applications. This material has not been explored in great depth in the literature, so little is known about its crack propagation behavior; the 3-D printed mesostructure of the material adds additional complexity to the problem. Simple finite element models of this mesostructure were created to demonstrate this and place the rest of the study in context. Three test articles were designed for 3-point-bend testing, each meant to test a different aspect of the crack development and growth. A desktop-sized testbed was designed and developed to test these articles. A series of six experiments were run, each of the test article designs in each of two print orientations. The six experiments were each replicated twice, for a total of 18 tests, to ensure repeatability and reliability of the collected data. The crack behavior overall seemed well captured using the developed experiment. Several potential improvements were identified and described. The validity of a linear-elastic, small-scale yielding assumption in the growth of cracks in PLA was also examined, as well as the crack velocity, crack stability, and fracture mode.

1 Background

Extrusion-based additive manufacturing, typically known as fused deposition modeling (FDM) is becoming more and more a fixture of modern design and manufacturing technology. Process optimization has been extensively studied, as well as material characterization for the various polymers processed using FDM. Figure 1 shows the basic process mechanics.

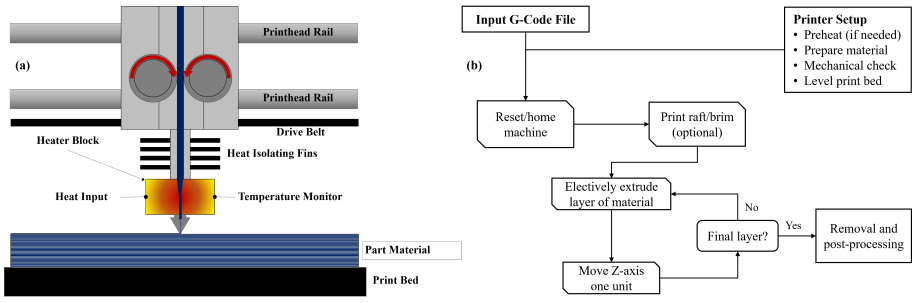

Figure 1: Fused deposition modeling (FDM) process [1]

The fracture behavior of extrusion-based 3-D printed materials has not been explored or researched in much depth. Some preliminary work has been done but has thus far been mostly limited to macro-scale testing of ABS samples and comparison to simple finite element models. Perez et al. [2]

looked in detail at the crack surface in tensile-tested ABS-based materials. The primary goal of the study was to discover the effect of various polymer additives on the crack surface characteristics; they found that the exact composition of the blend greatly affects the mechanical properties of the material and that the break pattern at the site of cracks demonstrated different failure modes which affected the properties. This was the only paper reviewed that discussed the mesostructure of the material. Patel & Patel [3] experimentally measured the stress intensity factors and crack tip opening displacements of a variety of ABS ASTM D5045-designed specimens with different crack lengths and build densities. This data was then used to build and tune a simple finite element model of the stress field around the crack. The authors of this study also provided a brief literature review of ABS mechanical properties, using this information as input into their FEM model; the FEM model did not consider the effects of the 3-D printed structure and seems to have assumed a continuum material. Patel et al. [4] was a similar study to [3], except specimens of different orientations were considered. Aliheidari et al. [5–8] have published several papers on optimizing FDM process parameters, such as print bed temperature, print speed, extrusion rate, and other characteristics. Some study of the adhesion between the layers was done on the mesoscale, but was not studied in great depth. Optimization of the process parameters specifically to cause crack dispersion was explored somewhat by Gardan et al. [9, 10], increasing the fracture toughness by 20-30%. The main contribution of this study is a method for steering the crack by orienting some of the printed fibers along principle stress directions.

None of the previous work found discussed the design possibilities, optimization, or design implications of FDM printed mesostructures nor discussed any materials other than ABS and various blends of which it is the main component. All of the mentioned studies examine the fracture toughness of ABS and various methods to improve it. No previous work was found concerning polylactic acid (PLA), another very commonly-printed polymer, or examining the crack tip propagation in the material. The present study seeks to examine this by introducing a set of 3-point-bend specimens, developing a test bed, and studying the crack propagation behavior of the material.

PLA is a very interesting and useful material and is commonly 3-D printed. It is a naturally-sourced form of polyester, is derived from plant matter, is compostable, and biodegradable. It has excellent mechanical properties and is a very stable polymer when used in its normal operating range of temperatures and environments [11, 12]. It is commonly used as a biocompatible material [13, 14]. Table 1.1 shows properties measured by the author for PLA in previous unpublished studies:

Table 1: PLA material properties

Property	**PLA**	**Units**
Elastic modulus (E)	2840	MPa
Yield strength (σ_y)	41.38	MPa
Ultimate strength (σ_u)	53.53	MPa
Testing temperature (T)	23.0	$^\circ C$
Density (ρ)	1250	kg/m^2

2 Finite Element Modeling of 3-D Printed Mesostructure

In order to understand the expected behavior of the realistic material, a set of elemental finite element models were built. Figure 2 shows the basic geometry, where a representative 1.5mm x 1.5mm x 0.8mm sample containing four layers was designed. The layers alternate directions, similar to realistic FDM-processed materials. A crack is cut into the element, cutting normal to the first and third layers and parallel to the second and fourth layers. This elemental specimen was then loaded in three different stress modes, as shown in Figure 3, and carefully meshed to ensure that both the fibers and their interfaces would be captures by a finite element (FEM) analysis. The three cases were then examined using FEM, the results of which are shown in Figure 4 as 3-D stress fields. Finally, the ISO fields (regions of constant stress) were calculated, as shown in Figure 5. It is very clear from this FEM analysis that the 3-D printed mesostructure of the materials has a very large influence on the stress fields within the element for all loading cases. These FEM models and results were produced using SolidEdge® and FEMAP®.

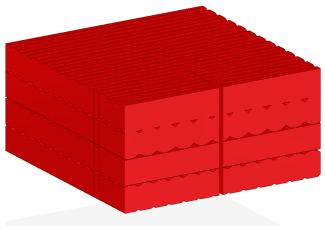

Figure 2: Element of FDM-printed mesostructure with pre-cut crack

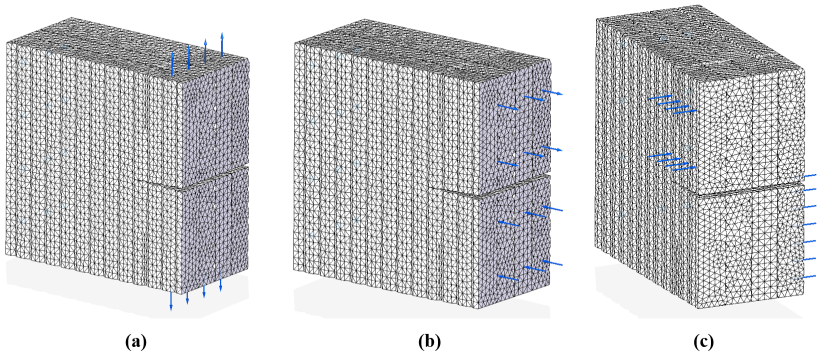

Figure 3: FEA mesh mesostructure for (a) Mode I, (b) Mode II, and (c) Mode III loadings

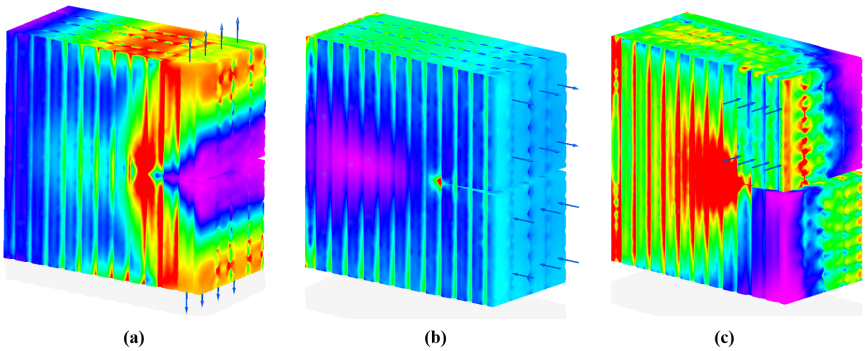

Figure 4: Stress fields for (a) Mode I, (b) Mode II, and (c) Mode III loadings

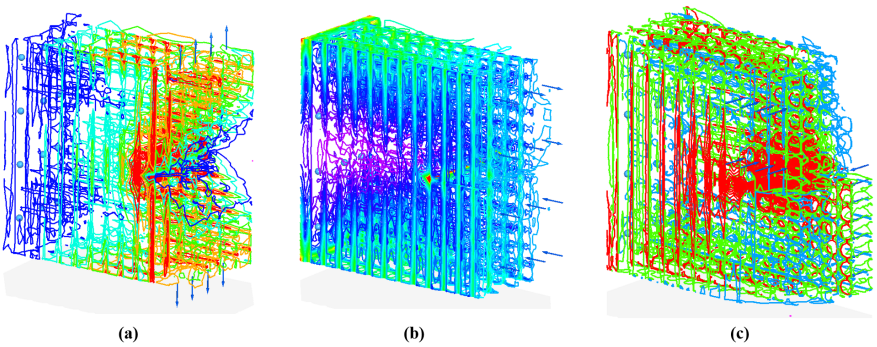

Figure 5: ISO (constant stress) fields for (a) Mode I, (b) Mode II, and (c) Mode III loadings

3 Materials & Methods: Test Article Design

3.1 Cracking in 3-D Printed Materials

The 3-point bend test on a single-crack bending specimen was selected as the test medium after a brief review of the available methods. This test is the typical standard for finding the fracture toughness of a material and the stress intensity factors, if the material characteristics are well-known [15, 16]. From the experience of the author in designing and using 3-D printed structures, there are three major failure areas in which cracks can start and propagate; in this section, a test article will be designed to explore and test each of these cases.

- The first, shown in Figure 6a, is cracking imitated in surface defects that do not involve breaking or cracking the strong part shell. These are usually caused by printing defects and incorrect tuning of the print process.
- The second, shown in Figure 6b, is the cracks that begin in the part shell and grow into the infill of a part that is not completely dense. These are commonly caused by rapid material cooling and residual stresses experienced by some materials.
- Finally, the third type of defect is cracking and delamination of parts that are printed as full-density parts (Figure 6c). This is typically caused by residual stresses and stress concentrations in the part after printing. Residual stressed affect full density parts more severely than partially-filled parts. Materials with high shrink rates upon cooling are most commonly affected by this.

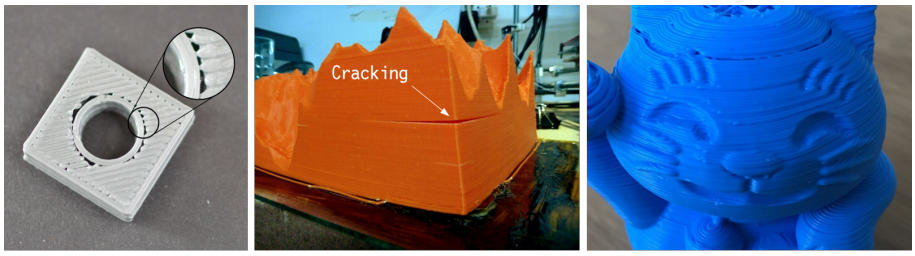

Figure 6: Cracking modes: (a) surface defects [17], (b) shell defects [18], and (c) delamination [19]

3.2 Design 1: 15% Shell with Cut

The first of the three test article designs explored the first cracking mode, the surface defect not involving the part shell. A 3-point bend specimen was designed as two parallel surfaces, each 0.8 mm thick and separated by an air pocket. A soft infill of 15% was used between the surfaces, enough to prevent bucking of the surfaces during the test but not enough to interfere with the crack propagation. A shell was used to contain the surfaces but was cut at the crack so that no shell was involved in the crack initiation or propagation. Figure 7 shows the setup and geometry. Figure 8 is a preliminary numerical 3-point bend test on the design to demonstrate the expected stress field in the sample during the bend test; red color indicates the yield stress of the material. For the physical test articles, the crack was sharpened using a $10\mu m$ engraving bit in a milling machine.

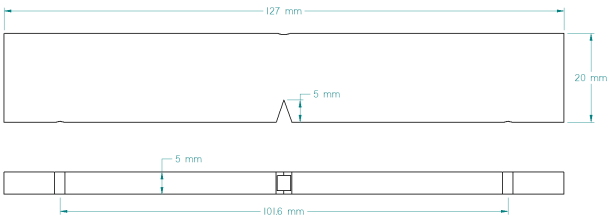

Figure 7: Design 1 geometry

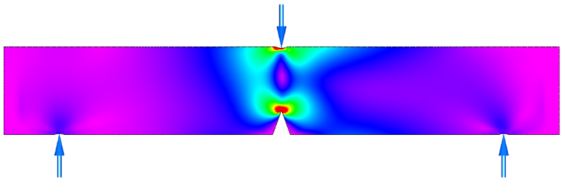

Figure 8: Design 1 FEM showing stress field

3.3 Design 2: 15% Shell Without Cut

The design for the shell-cracking mode was identical to Design 1, except that the shell was included in the crack. The crack must pass through the hard part shell before reaching the 0.8mm-thick surface inside. Figures 9 and 10 show the geometry and FEM analysis of this configuration.

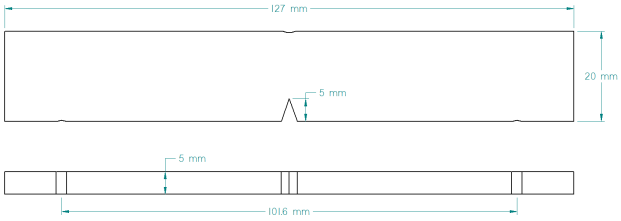

Figure 9: Design 2 geometry

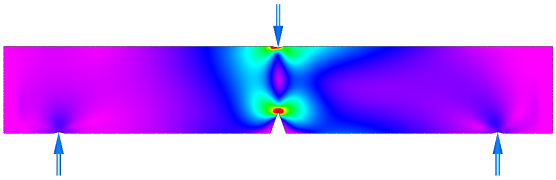

Figure 10: Design 2 FEM showing stress field

3.4 Design 3: 100% Infill with Shell

Design 3 was printed full-density. In addition, the sample was made thinner and the crack made longer so that any plasticity effects could be more easily observed. Figures 11 and 12 show the geometry and initial FEM 3-point test. The red region near the crack tip indicates the area above the yield stress of the material.

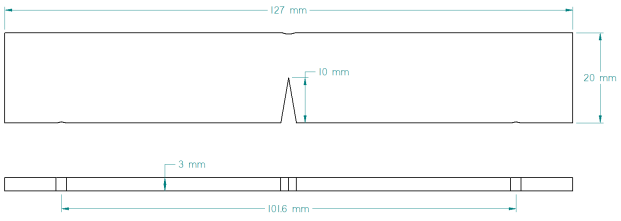

Figure 11: Design 3 geometry

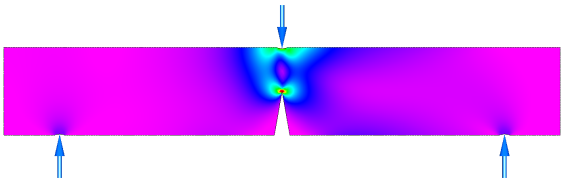

Figure 12: Design 3 FEM showing stress field

4 Materials & Methods: Test Bed Design

The second part of the present experiment, after the design of test articles, was the development of a test bed for performing the experiments. The 3-point bend test is commonly done using a universal testing machine. However, the decision was made to design and build a dedicated test bed because

1. A universal testing machine with the needed control and accuracy was not available
2. A desktop-sized test bed that can be stabilized and used for many experiments will be very useful for the current and future experiments.
3. Developing a simple open-source test bed will be useful to the advancement of open scientific instruments

Figure 13 shows the basic layout of the developed test bed. Component (A) is the driver for the system, consisting of a driver motor, a tensioner, and driven screw which advances the jaws of the 3-point bend system; the drive belt is a GT-2 rubber-glass fiber composite timing belt. Component (B) is the set of pressure points for the 3-point test; the upper jaw (center force point) is driven by the drive motor and the lower two points are fixed. Component (C) is the crack-tracking camera, consisting of a GoPro camera set to a high frame rate and augmented with a 6-layer microscopic lens for focus; the lens is protected via the red hard shell. Component (D) is the force measuring system, consisting of a specially-designed load cell; this will be discussed in more depth later. Component (E) is the lighting system; the basis of this system is a pair of LED off-road truck spotlights attached to a switch and a 12V SLA battery. Finally, component (F) is the basic frame of the system, which is a cast iron machinist clamp augmented with other parts to create the 3-point bend frame. Detailed views of major parts of the design are shown in Figures 14-16.

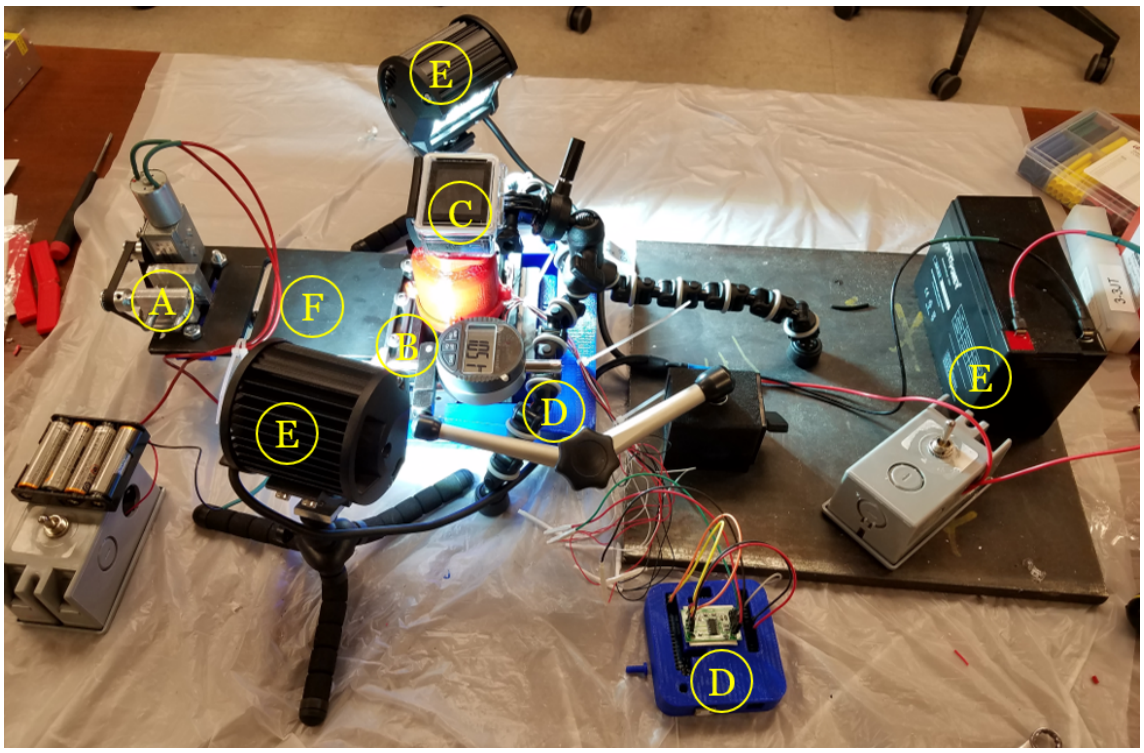

Figure 13: Desktop 3-point bend test bed

Figure 14a is the data acquisition system, consisting of a GoPro camera with microscopic lens attachment and a digital displacement indicator; as the 3-point jaws close and the sample is bent, the indicator gives the distance traveled at a tolerance of 0.01mm. The jaws of the 3-point bend tester are shown in Figure 14b. The basic frame of the tool, both the upper and lower jaws, were machined from aluminum. The contacting points were made from mild steel and attached to the

main tool via press fit and steel-fiber reinforced epoxy. The upper jaw (single point) is bolted directly to the machinist clamp, while the lower jaw (two points) slides in a track and interfaces with the clamp through a bank of load cells which measure the force applied to the specimen. The tooling was well-oiled and checked for smooth operation, stability, and low friction before use.

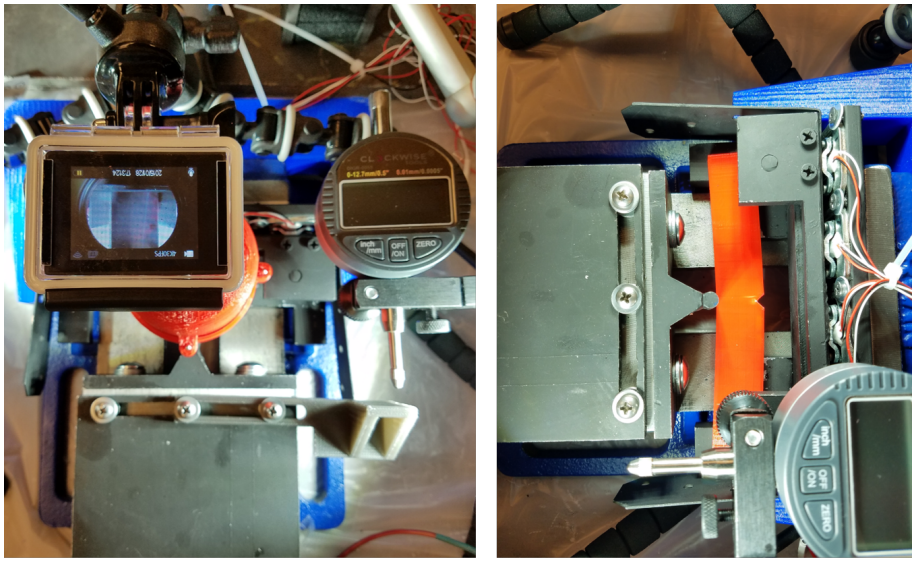

(a) **(b)**

Figure 14: Test bed detail views: (a) data acquisition system and (b) 3-point bend jaws

Figure 15 shows the detail of the force-measuring system. A set of half-bridge cantilever beam load cells were configured in a set of four to create a Wheatstone bridge, where the strain gauges on the load cells serve as the resistors in the bridge. This configuration is much more accurate than most load cell measurements, due mainly to the high resolution of the readings and the ability to tune the load cell output to ensure accuracy. The configuration shown has a maximum operating load of 1950N.

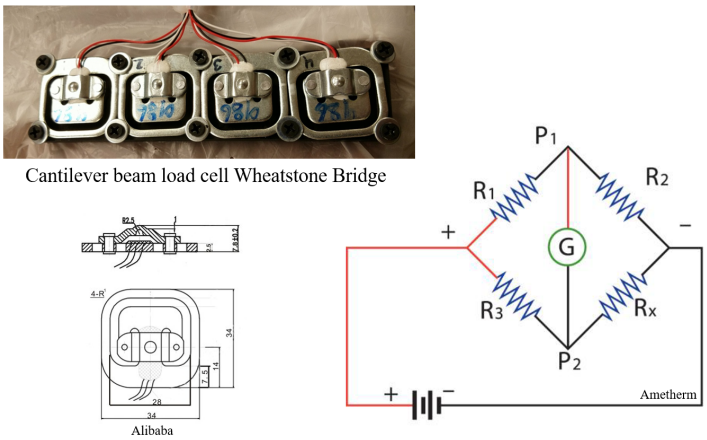

Figure 15: Load cell configuration

Figure 16a shows the drive system, which includes a drive motor, a tensioner, and a driven screw which advances the upper (single point) jaw to bend and crack the specimen. The motor is a 5-6V tool motor spinning at 1750rpm, which is geared down for an output speed of 0.5rpm. The output gear has 20 teeth, while the driven gear has 30 teeth to provide a larger grip surface for the GT-2 timing belt. The drive screw has a thread pitch of 13 threads/inch, giving an operating speed of 0.65 mm/min. Different gears and a motor speed governor could be used to modify this strain rate, if needed. Finally, Figure 16b shows the circuit for reading the load cells and collecting the

data. It consists of an Arduino board, a converter/amplifier (shown in blowup window), and a laptop. The entire unit is powered by the 5V power supply on the laptop and supplied through the USB cable.

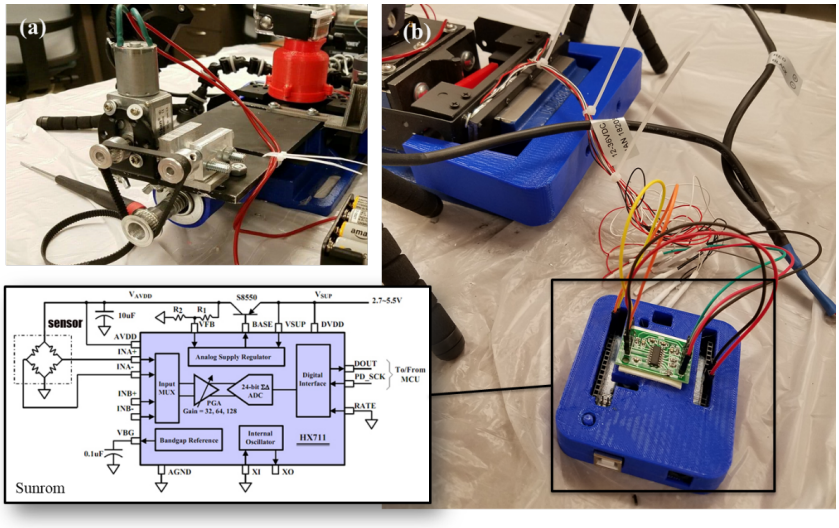

Figure 16: (a) Drive system and (b) detail of data acquisition system

5 Experimental Setup

The experimental setup was relatively simple, consisting of 3-point bend tests on the three test articles designed in Section 3. To briefly explore the effect of print orientation, two different orientations were tested, parallel to crack and perpendicular to crack, as shown in Figure 17. The printing configuration for each is shown in Table 2 below. The experiment was run three times to test the consistency and replicability of the results. The basic configuration and approach of the 3-point bend test shown in Figure 18 was followed. Each study recorded the force-deflection curve and the crack length with respect to time. The crack length was captured on camera using small strips of paper with 0.5mm tick marks glued along the crack; initial tests attempted to use computer vision tools to capture the crack tip, but the contrast between the crack and the surrounding material was too low for the program to detect the crack.

Table 2: Printing parameters

Material	$\boldsymbol{T_{print}}$ $(^\circ C)$	$\boldsymbol{T_{bed}}$ $(^\circ C)$	$\boldsymbol{v}$ (mm/s)	**Nozzle**	**Shell** (mm)	**Printer**
PLA	205	70	60	0.4 mm brass	0.80	Prusa i3

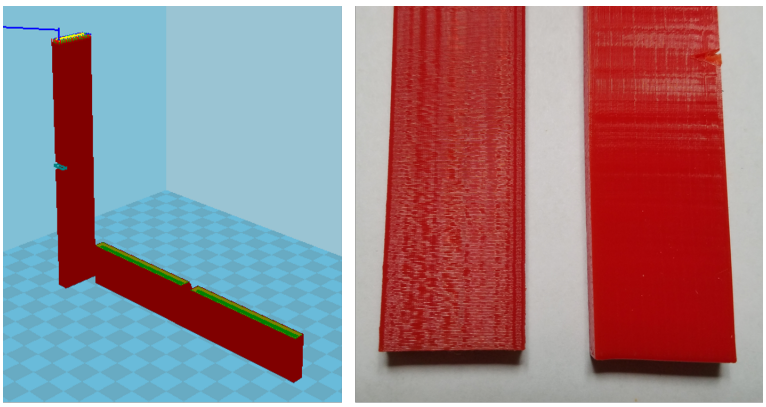

(a) **(b)**

Figure 17: (a) CURA pre-processing and (b) finished samples in the shown orientations

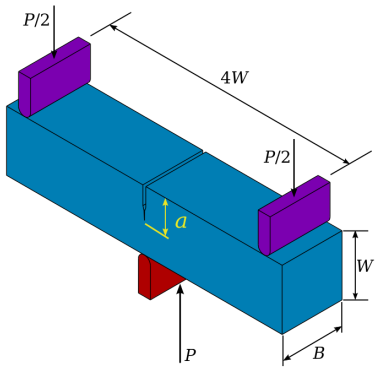

Figure 18: 3-point bend test setup and configuration [20]

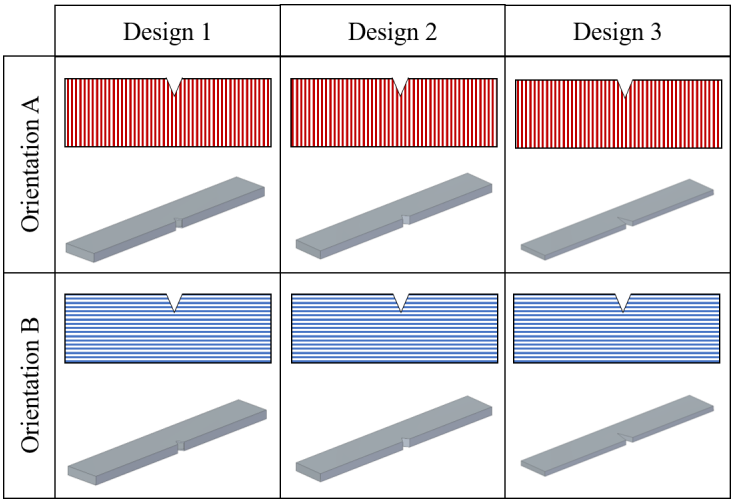

Figure 19: (a) CURA pre-processing and (b) finished samples in the shown orientations

Figure 19 shows the configurations of each of the studies, given three sample designs and two orientations for each. The tests were named according to their combination of design and orientation; for example, the first test (upper left) shown in Figure 19 would be labelled "Test 1A". These names are appended with the replication name, for example "Test 1A1" for Design 1, Orientation A, Replication 1.

6 Experimental Results

This section presents the raw results taken from the experiment described in Section 5. Figures 20 and 21 are the force-time curves for the 6 orientations, the red curves being Replication 1, the blue Replication 2, and yellow Replication 3 of the same configuration. Since a constant strain rate was used, these plots also represent the force-deflection curves. Below each of the plots, the crack tip at an arbitrary point in the cycle is shown; the crack tip for Experiment 2A was not able to be captured for any of the three runs due to the sudden and complete failure of the parts with no advance crack growth. Figures 22-23 show the crack propagation in the samples with respect to time under constant strain rate described previously. As previously discussed, the samples for Study 2A were not able to be captured by the experiment do to extremely rapid failure. However, all of the other results were captured well. It is clear from the stair-step nature of the crack growth plots that the fibers in the material must break for the crack to grow; in many cases, the crack simply arrests naturally until additional energy is placed on the material to cause further growth. This is particularly obvious in Studies 1B-3B where the crack must travel perpendicular to the surface fiber direction (Figure 21). Screen shots of the video recorded of the crack propagation is shown below each of the plots.

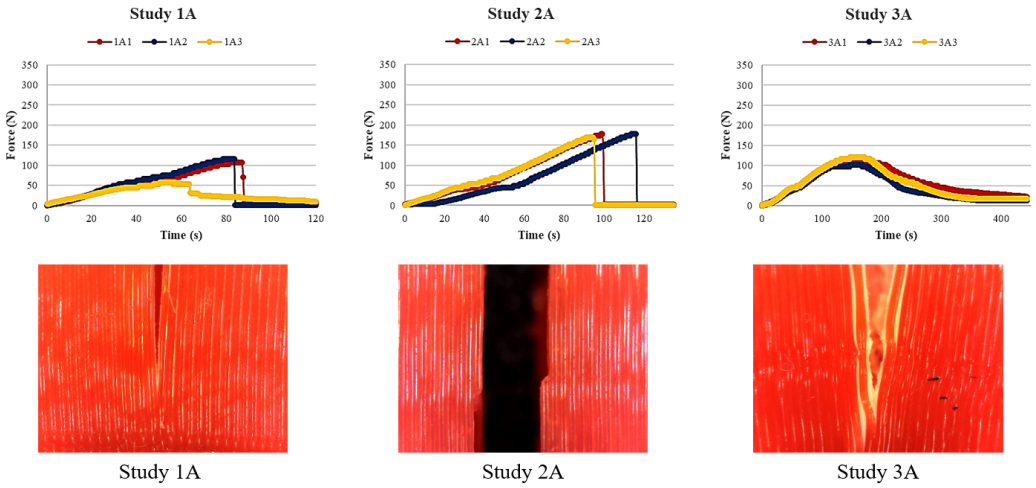

Figure 20: Tests 1A-3A results

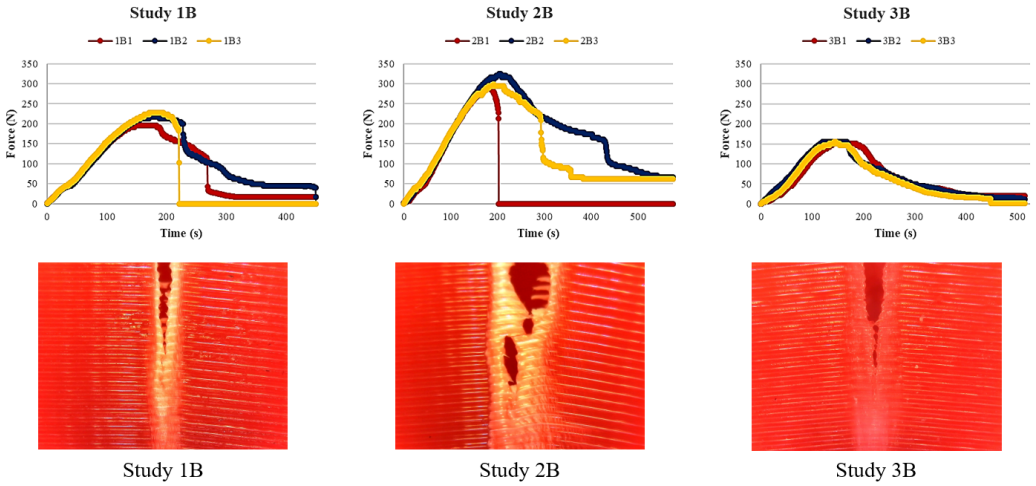

Figure 21: Tests 1B-3B results

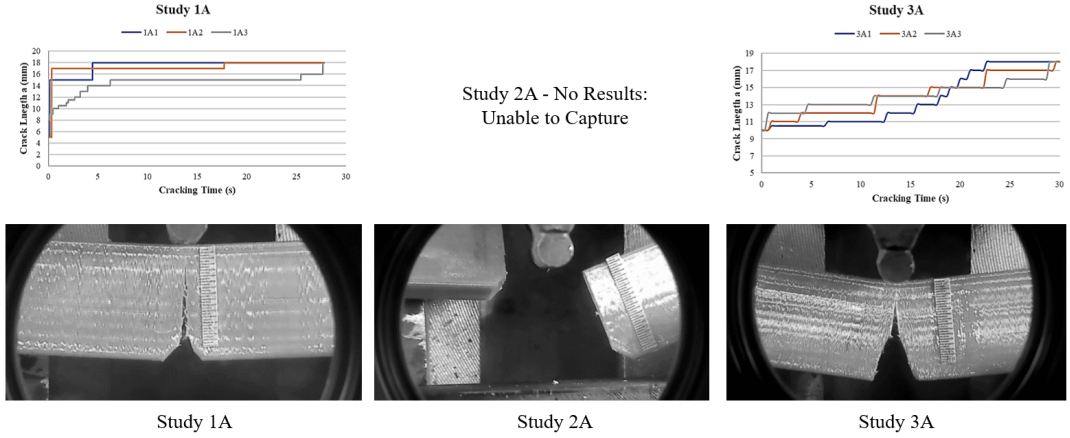

Figure 22: Study 1A-3A crack growth results

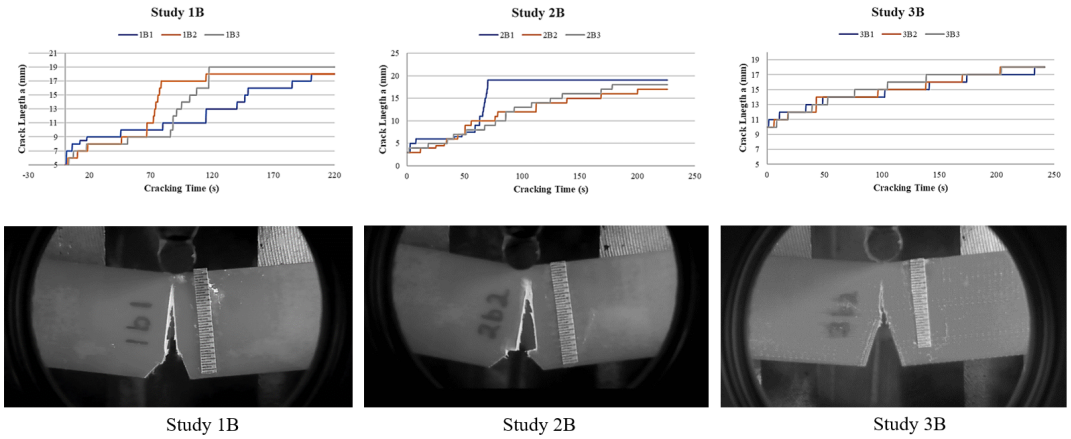

Figure 23: Study 1B-3B crack growth results

7 Discussion and Conclusions

In the present study, six different cases were explored to gain some preliminary insight into the crack propagation behavior of the 3-D printed PLA material. The three different test articles designed tested the propagation of the crack from three common failure modes in macro-scale 3-D printed parts. A number of important considerations and observations are discussed in this section.

Small-scale yielding assumption: The first and most important assumption that was made was the assumption of elasticity with small-scale yielding; the test articles and the test bed were designed with this assumption in mind. Now that some preliminary results have been found, it is important to check the validity of this assumption in the actual tests. For an isotropic linear-elastic material, a look at the plots in Figure 20 and 21 would provide an answer to this question; however, in this case the failure involves potentially hyper-elastic materials and fiber failure during crack propagation. The material used in this study, PLA, has a very interesting and fortunate property that can be examined to study the question of small scale yielding: it changes color when plastically deformed. This study used dark red PLA, which shows excellent color-changing properties. Figure 24 shows an example that was specially made to demonstrate the property; Figure 24a shows the undamaged specimen and Figure 24b shows the plastic zone ahead of a crack tip. The length scale in this figure is five lines/ridges per millimeter.

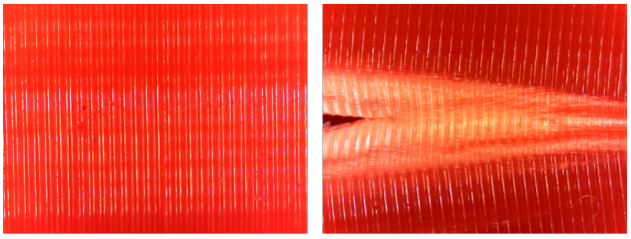

Figure 24: Demo of color-changing under plasticity in PLA

By definition, small scale yielding occurs when the plastic zone is very small compared to the rest of the sample, it is located only near the crack tip, and does not affect the boundaries of the sample [21–23]. All of the samples were checked, and none displayed a plastic wake thicker than 0.5mm or in a location far from the crack tip itself. Therefore, it is reasonable to conclude that the material does indeed fail under a small-scale yielding condition. Examining the cracks in the experimental samples, and illustrated by Figure 24b, the shape of the plastic zone seems to indicate that the material is nonlinear elastic (like rubber) and that the cracks formed as they would in an epoxy or rubber material [24]. Figure 25 shows some published research results that seem to match the behavior of the 3-D printed PLA material.

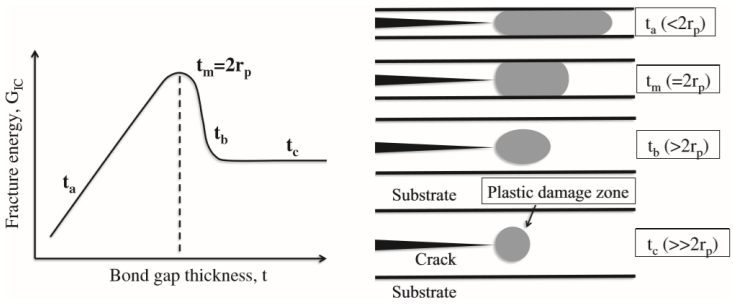

Figure 25: Results for fracture of elastic epoxy from Quan et al. [24]

Crack stability: Crack stability is an important consideration. The stability of the crack growth was recorded during the experiments and, with the exception of experiment 2A, the cracks were found to be very stable. In all cases, the crack stopped growing naturally and required additional energy input from the 3-point bend test to continue growing. This phenomenon is obvious in the plots shows in Figures 22 and 23.

Fracture mode of material: One of the most interesting things observed during the present experiment is that, even under 3-point bending (Mode I) condition, there is still an internal anti-plane shear (Mode III) condition present. The Mode I condition comes from the bending of the specimen and the resulting breakage of the material fibers; the Mode III condition seems to come from the sliding of the planes of fibers relative to each other due to anisotropic material strength. Figure 26 shows some results from a preliminary version of the present experiment, where this combined fiber failure and plane sliding was observed (note the surface stretch marks in Figure 26a). The main experimental samples did not show this effect nearly as dramatically in the failed samples (Figures 23 and 24b show some evidence), but likely would if they were thicker. This effect needs to be further investigated in future work in this area.

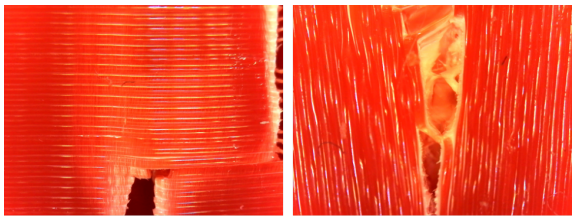

Figure 26: Observations of combined Mode I/Mode III fracture activity

Crack velocity: The calculation of the mean crack velocity will give much insight into the fracture behavior of the material, essentially providing a regression line of crack length with respect to time. This will give a good method for calculating the energy released by the crack as it propagates [16]. Unfortunately, this experiment did not give enough data to be able to calculate this rigorously, but this will be addressed in future work in this area. The mesostructure of the material will likely have a very strong impact on the crack velocity.

References

[1] S. L. Messimer, A. E. Patterson, N. Muna, A. P. Deshpande, and T. R. Pereira, "Characterization and processing behavior of heated aluminum-polycarbonate composite build plates for the FDM additive manufacturing process," *Journal of Manufacturing and Materials Processing*, vol. 2, no. 1, p. 12, 2018.

[2] A. R. T. Perez, D. A. Roberson, and R. B. Wicker, "Fracture surface analysis of 3d-printed tensile specimens of novel ABS-based materials," *Journal of Failure Analysis and Prevention*, vol. 14, no. 3, pp. 343–353, 2014.

[3] N. D. Patel and B. B. Patel, "Fracture analysis of fdm manufactured acrylonitrile butadiene styrene using FEM," *International Journal of Recent Research in Civil and Mechanical Engineering*, vol. 2, no. 1, pp. 84–90, 2015.

[4] R. Patel, H. Shah, and S. V. Kumari, "Experimental investigation of fracture of ABS material by ASTM D-5045 for different crack length & layer of orientation using FDM process," *International Journal of Mechanical and Industrial Technology*, vol. 3, no. 1, pp. 79–83, 2015.

[5] N. Aliheidari, R. Tripuraneni, C. Hohimer, J. Christ, A. Ameli, and S. Nadimpalli, "The impact of nozzle and bed temperatures on the fracture resistance of FDM printed materials," in *Behavior and Mechanics of Multifunctional Materials and Composites 2017* (N. C. Goulbourne, ed.), SPIE, 2017.

[6] N. Aliheidari, R. Tripuraneni, J. Christ, A. Ameli, and S. Nadimpalli, "Measuring the interlayer fracture resistance of fdm printed thermoplastics," in *Conference: Conference: Society of Plastics Engineers, Annual Technical Conference SPE-ANTEC, At Indianapolis, Indiana*, 2016.

[7] N. Aliheidari, R. Tripuraneni, J. Christ, A. Ameli, and S. Nadimpalli, "Fracture toughness of fused deposition modeled thermoplastics," in *Conference: 53rd Annual Technical Meeting of the Society of Engineering Science, At Maryland*, 2016.

[8] N. Aliheidari, J. Christ, A. Ameli, R. Tripuraneni, and S. Nadimpalli, "Optimizing fused deposition modeling 3d printing process for fracture resistance," in *SPE ANTEC Anaheim 2017*, 2016.

[9] J. Gardan, A. Makke, and N. Recho, "A method to improve the fracture toughness using 3d printing by extrusion deposition," *Procedia Structural Integrity*, vol. 2, pp. 144–151, 2016.

[10] J. Gardan, A. Makke, and N. Recho, "Improving the fracture toughness of 3d printed thermoplastic polymers by fused deposition modeling," *International Journal of Fracture*, vol. 210, no. 1-2, pp. 1–15, 2017.

[11] L.-T. Lim, R. Auras, and M. Rubino, "Processing technologies for poly(lactic acid)," *Progress in Polymer Science*, vol. 33, no. 8, pp. 820–852, 2008.

[12] M. A. Cuiffo, J. Snyder, A. M. Elliott, N. Romero, S. Kannan, and G. P. Halada, "Impact of the fused deposition (FDM) printing process on polylactic acid (PLA) chemistry and structure," *Applied Sciences*, vol. 7, no. 6, p. 579, 2017.

[13] U. Ritz, R. Gerke, H. Götz, S. Stein, and P. M. Rommens, "A new bone substitute developed from 3d-prints of polylactide (PLA) loaded with collagen I: An in vitro study," *International Journal of Molecular Sciences*, vol. 18, no. 12, p. 2569, 2017.

[14] K. Immonen, P. Lahtinen, and J. Pere, "Effects of surfactants on the preparation of nanocellulose-PLA composites," *Bioengineering*, vol. 4, no. 4, p. 91, 2017.

[15] G. V. Guinea, J. Planas, and M. Elices, "Measurement of the fracture energy using three-point bend tests: Part 1—influence of experimental procedures," *Materials and Structures*, vol. 25, no. 4, pp. 212–218, 1992.

[16] J. Loya, E. Villa, and J. Fernández-Sáez, "Crack-front propagation during three-point-bending tests of polymethyl-methacrylate beams," *Polymer Testing*, vol. 29, no. 1, pp. 113–118, 2010.

[17] "Print quality troubleshooting." Website available at https://www.simplify3d.com/support/print-quality-troubleshooting/. Accessed: 2017-11-21.

[18] "Comprehensive Introduction to 3D Printing Technology." Website available at http://3dprintingforbeginners.com/a-comprehensive-introduction-to-3d-printing-technology/. Accessed: 2017-11-21.

[19] "Troubleshooting guide to 19 common 3d printing problems." Website available at http://www.geeetech.com/blog/2016/12/troubleshooting-guide-to-19-common-3d-printing-problemspart-one/. Accessed: 2017-11-25.

[20] "Three-point flexural test." Website available at https://en.wikipedia.org/wiki/Three-point_flexural_test. Accessed: 2017-11-21.

[21] G. Irwin, "Analysis of stresses and strains near the end of a crack traversing a plate," *Journal of Applied Mechanics*, vol. 24, pp. 361–364, 1957.

[22] J. Rice, "Limitations to the small scale yielding approximation for crack tip plasticity," *Journal of Mechanics and Physics of Solids*, vol. 22, pp. 17–26, 1974.

[23] J. Thomas, K. Koppenhoefer, and J. Crompton, "Small scale yielding model for fracture mechanics," in *Proceedings of the 2014 COMSOL Conference, Boston, MA.*, 2016.

[24] D. Quan, N. Murphy, and A. Ivankovic, "Fracture behaviour of epoxy adhesive joints modified with core-shell rubber nanoparticles," *Engineering Fracture Mechanics*, vol. 182, pp. 566–576, 2017.